High-resolution timing of cell cycle-regulated gene expression

Maga Rowicka*, Andrzej Kudlicki*, Benjamin P. Tu, and Zbyszek Otwinowski*

Department of Biochemistry, University of Texas Southwestern Medical Center, 5323 Harry Hines Boulevard, Dallas, TX 75390

Communicated by Steven L. McKnight, University of Texas Southwestern Medical Center, Dallas, TX, June 27, 2007 (received for review February 23, 2007)

The eukaryotic cell division cycle depends on an intricate sequence of transcriptional events. Using an algorithm based on maximum-entropy deconvolution, and expression data from a highly synchronized yeast culture, we have timed the peaks of expression of transcriptionally regulated cell cycle genes to an accuracy of 2 min (≈1% of the cell cycle time). The set of 1,129 cell cycle-regulated genes was identified by a comprehensive analysis encompassing all available cell cycle yeast data sets. Our results reveal distinct subphases of the cell cycle undetectable by morphological observation, as well as the precise timeline of macromolecular complex assembly during key cell cycle events.

mitosis | microarrays | yeast | maximum entropy

Eukaryotic cell division is a complex process, with many layers of regulation at the level of gene transcription, protein production, localization, modification, and degradation. Many genes specific to the cell cycle are regulated transcriptionally (1–5) and are expressed just before they are needed (6). The precise determination of the moment of maximum expression is, therefore, important for understanding the cell division process. The timing of gene expression is also an important factor in various analyses of gene coexpression networks, evolution of regulation, global organization of transcription, inferring transcription factor specificities, and many other analyses (7–11).

Previous whole-genome studies of the yeast cell cycle relied on microarray data from artificially synchronized cultures grown under nutrient-rich laboratory conditions (1, 3, 5). Under these typical conditions, cell divisions happen immediately, one after another, with almost overlapping cell division phases, thereby hindering accurate timing [see supporting information (SI) *Appendix*]. Moreover, Fourier methods have typically been used for timing of genes (3, 5, 8), but these methods are limited to genes with one expression peak per cycle and are most accurate for temporal profiles resembling a sinusoid. A model-based approach to timing was also developed (12), but it remained unable to deal with multiple peaks or to achieve a high temporal resolution. Because of these experimental and methodological limitations, the timing of the cell cycle transcriptional program by using logarithmically growing yeast and Fourier methods (3, 5, 13) lacks within-phase resolution (i.e., the variance of expression peaks of individual genes is comparable to the lengths of cell cycle phases; see *SI Appendix*). The timing of gene expression by using such data and methods, therefore, is not interpretable beyond assigning transcripts to main cell cycle phases in which their expression peaks: G_1 (gap 1), S (DNA synthesis), G_2 (gap 2), M (mitosis), and M/G_1 (1, 5).

Here we present a unique approach to the timing of cell cycle-regulated gene expression. We rely on a recent data set, in which a naturally synchronized continuous yeast culture proceeds through ≈5-h metabolic cycles (yeast metabolic cycle; YMC) (14) while exhibiting strong and stable cell cycle synchronization. Using the characteristic profile shape of regulated genes (Fig. 1) to align cell cycles of the whole culture by maximum-entropy deconvolution, we reveal a high-resolution timeline of cell cycle transcriptional events in fine detail.

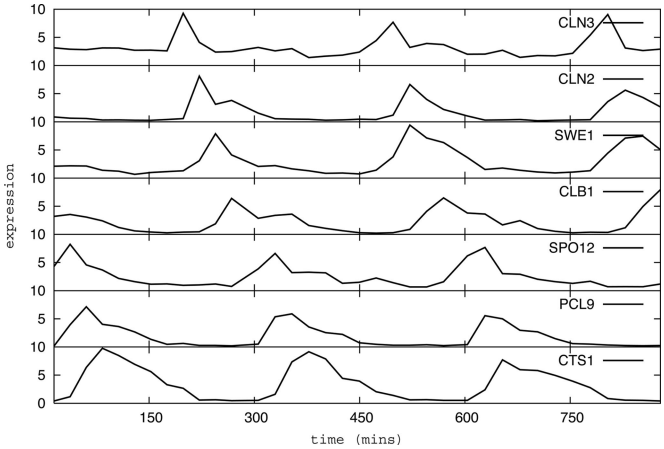

Fig. 1. Characteristic temporal profile of cell cycle-regulated genes. Presented are the raw expression data (14) of several transcripts that peak at different times: cyclins (*CLN3*, *CLN2*, *CLB1*, and *PCL9*); a Cdc28p inhibitor (*SWE1*); a positive regulator of mitotic exit (*SPO12*); and an endochitinase, crucial for cell separation after mitosis (*CTS1*). *y* axis, normalized expression (arbitrary units); *x* axis, time in minutes.

Results

Timing. The recent YMC expression data (14) exhibit strong modulation of cell cycle-regulated genes in a budding yeast culture (see SI Fig. 5). On examining the temporal expression profiles of the YMC data set, we calculated (15) that the average peak-to-trough expression ratio of the 108 well known cell cycle-regulated genes (see Table 3 in *SI Appendix*) is 21, compared with <9 for earlier synchronization by *cdc15* or *cdc28* temperature-sensitive mutants or by alpha pheromone (1, 5). Unlike the previous data (1, 3, 5), derived from rapidly growing yeast, the YMC data are collected from a continuous, highly synchronized, slowly growing yeast culture (14), which allows us to better distinguish peaks of some key cell cycle genes (Fig. 2). Furthermore, the initial synchronization of cells undergoing the YMC is achieved simply by starving the cell population after it reaches high density; this approach does not rely on the use of temperature-sensitive mutants, the addition of

Author contributions: M.R. and A.K. contributed equally to this work; M.R., A.K., B.P.T., and Z.O. designed research; M.R., A.K., and Z.O. performed research; M.R., A.K., B.P.T., and Z.O. contributed new reagents/analytic tools; M.R. and A.K. analyzed data; and M.R., A.K., B.P.T., and Z.O. wrote the paper.

Conflict of interest statement: S.L.M. declares a conflict of interest (such as defined by PNAS policy). ''The manuscript titled 'High-resolution timing of cell cycle-regulated gene expression' is coauthored by a group of scientists working in the Department of Biochemistry that I chair here at University of Texas Southwestern Medical Center. I am highly familiar with the research because it makes extensive use of data coming from my own laboratory.''

Abbreviations: CCTR, cell cycle transcriptionally regulated; SPB, spindle pole body; YMC, yeast metabolic cycle.

*To whom correspondence may be addressed. E-mail: zo@work.swmed.edu, andrzej@work.swmed.edu, or maga@work.swmed.edu.

This article contains supporting information online at www.pnas.org/cgi/content/full/0706022104/DC1.

www.pnas.org/cgi/doi/10.1073/pnas.0706022104

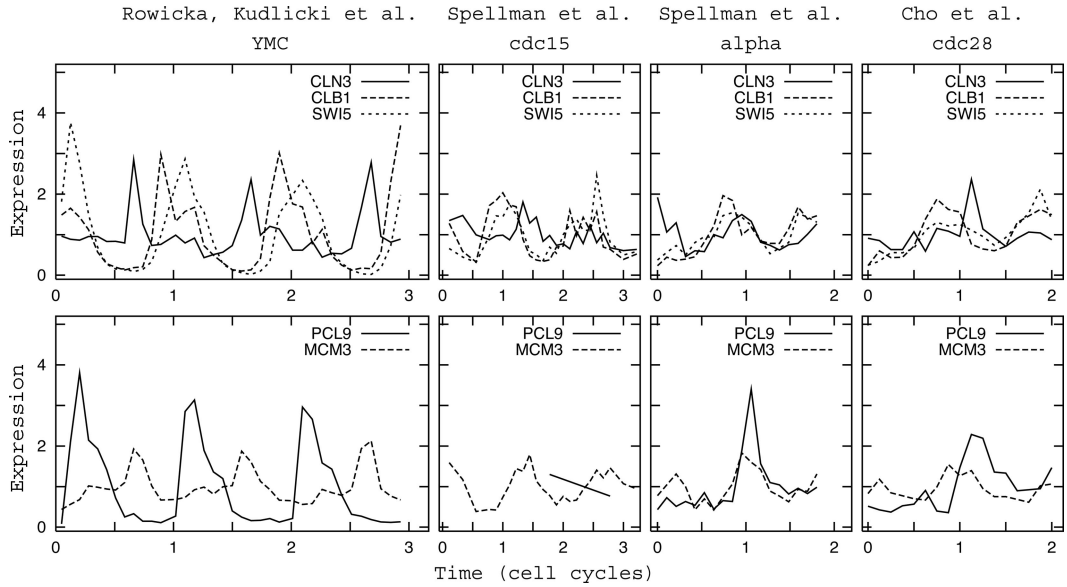

Fig. 2. Comparison of expression patterns of key cell cycle-regulated genes in slowly growing [YMC (14), *Left*] vs. rapidly growing [cdc15, alpha, and cdc28 (1, 5)] yeast cultures. (*Upper*) G_2 cyclin *CLB1*, mitotic transcription factor *SWI5*, and G_1 cyclin *CLN3*. (*Lower*) Mitotic cyclin *PCL9* and MCM subunit *MCM3*. Environment-dependent G_1 phase is ≈10 times longer in YMC than found in previous studies (cdc15, alpha, and cdc28 synchronization), allowing the expression of key cell cycle genes to be timed with higher accuracy.

pheromone, etc. The metabolically achieved synchrony (14) thus remains remarkably stable; it has lasted for ≈100 cycles, whereas synchronization achieved by other methods deteriorates noticeably during the first three cycles (5). The stable repetition of temporal expression patterns over consecutive cycles is an essential requirement for applying our deconvolution-based, accurate timing method. Therefore, we chose to base high-resolution timing solely on the YMC data (14), whereas other data sets (1, 3, 5) were used for identification of the set of cell cycle transcriptionally regulated (CCTR) genes.

We observed that most genes known to be transcriptionally regulated during the cell cycle share a characteristic profile shape in the YMC data (Fig. 1). On the basis of fluorescence-activated cell sorting (FACS) analysis of DNA replication and the observation of bud appearance (14), we conclude that the observed broadness of the profile is caused not by long transcript lifetimes but by individual cells entering the cell cycle at different times. To correct for the influence of this spread on measured mRNA concentrations, we modeled the time-shift distribution of cells entering the cell cycle (see *SI Appendix*). The shape of that distribution is strikingly similar to the budded cell count distribution from other cell cycle-synchronized cultures (1), suggesting that this shape is an inherent property of the cell cycle, likely caused by daughter cells needing more time than mother cells to grow big enough to divide again (16, 17).

To recover the mRNA concentration in the typical individual cell, we deconvolved the measured profile by using the common shape. The intrinsic noise in budding yeast gene expression is low (18), so we expect our estimated average individual cell expression timing to be reflective of the majority of actual single cells. We implemented a deconvolution algorithm adapted to microarray data analysis (see *SI Appendix*), with regularization based on the maximum-entropy principle (19). We thus accurately determined the moment of the gene expression peak by aligning cell cycles of the whole culture by deconvolution of the observed expression profiles (see *SI Appendix*). This method allows the recovery of single cell expression profiles, which in the microarray measurement are distorted because of averaging mRNA levels of imperfectly synchronized cells (Fig. 3).

Expression Peaks. For each transcript, we calculated the deconvolved profiles (see SI Fig. 7) and identified the peaks of expression (see *SI Appendix*). Deconvolution of gene expression profiles allows the discovery of secondary expression peaks, even when they are not evident in the raw data. Indeed, we find that many CCTR genes may peak twice per cycle. For example, deconvolved profiles of histone genes show that all histones except *HTB2* are expressed in two distinct bursts per cycle (SI Fig. 8): the first occurring in S phase and related to DNA

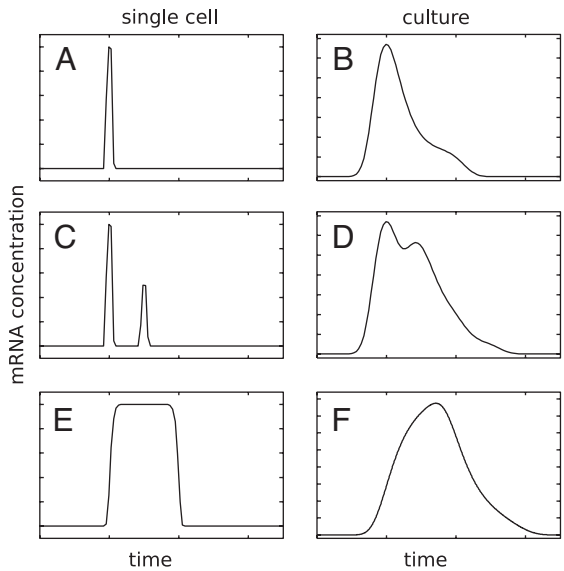

Fig. 3. Expression profiles measured for the whole culture differ considerably from single-cell mRNA profiles. Imperfect synchronization of cells results in broadening of expression profiles measured in the culture (*Right*), compared with the respective single-cell profiles (*Left*). The original single-cell expression profiles (*A*, *C*, and *E*) can be reconstructed from the observed profiles (*B*, *D*, and *F*, respectively) by using deconvolution. This method can also be applied when the single-cell expression profile is complex (*C* and *E*) rather than just one short-lived pulse (*A*).

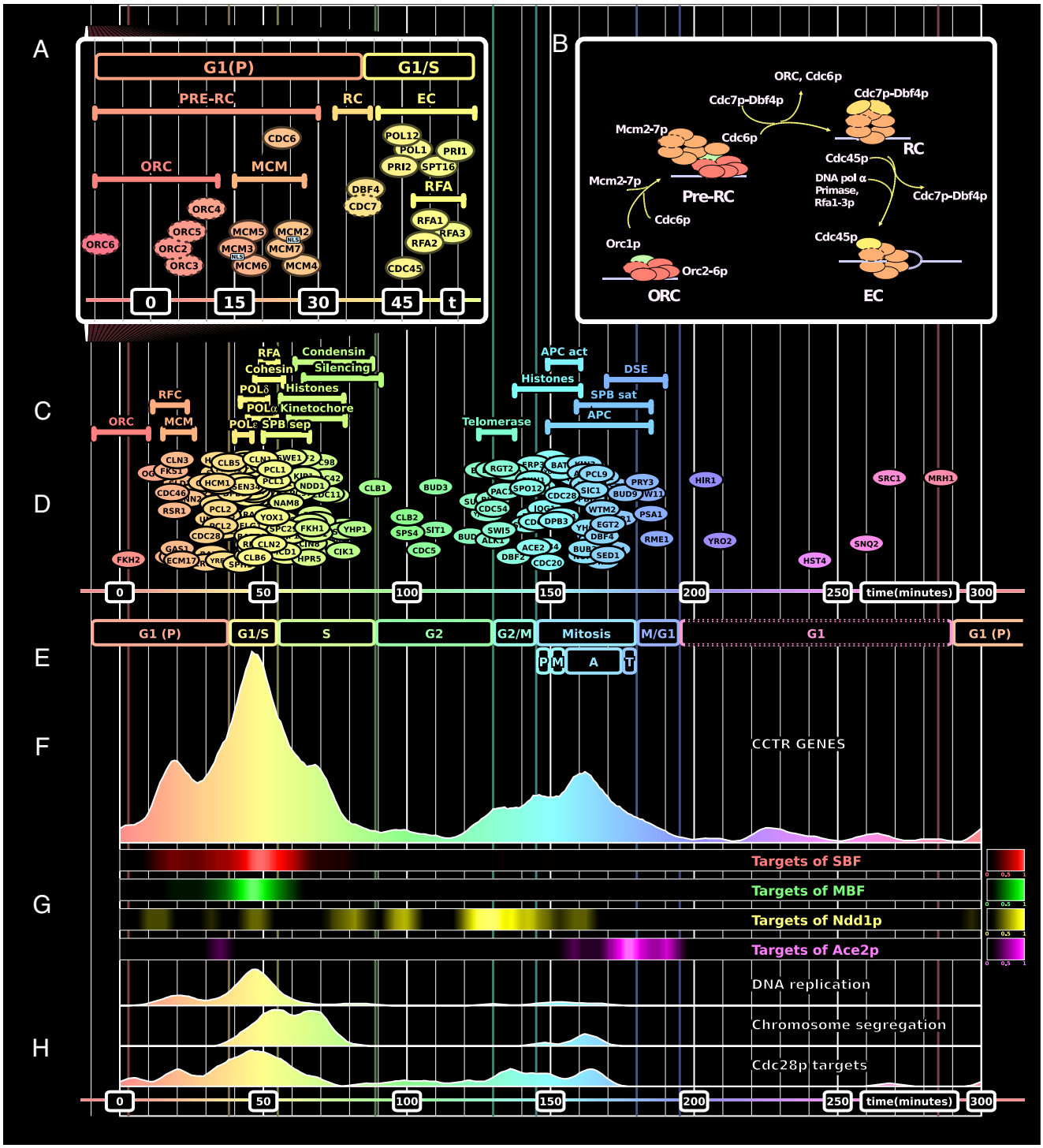

Fig. 4. Transcriptional program of the yeast cell cycle. (*A* and *B*) Proteins involved in DNA replication initiation, color-coded according to timing of their expression. The prereplication complex (pre-RC) undergoes several changes before an elongation complex (EC), capable of initiating DNA synthesis, is formed (24). The order of expression (*A*) agrees with the order in which gene products are needed (*B*). In *A*, dotted outlines denote non-CCTR genes. Note the two groups of MCM subunits, each containing one nuclear localization signal (NLS). In B, solid outlines denote primary expression peak; dashed outlines denote secondary (lower scoring) peak. The only exception to just-in-time transcription is *ORC1*. (*C*) Timing of CCTR complexes. DSE, daughter-cell-specific expression program; APC act, APC activation; SPB sat, spindle pole body satellite formation; SPB sep, spindle pole body duplication and separation. (*D*) Peaks of selected CCTR genes. (*E*) Phases and subphases of the cell cycle. Note new prereplicative G_1 (P) phase. (*F*) Histogram of expression peaks of CCTR genes. (*G*) Peaks of transcripts regulated by selected cell cycle transcription factors (11, 20, 21, 29, 30). Note the differences in expression of MBF and SBF targets. (*H*) Histograms of peaks of CCTR genes involved in selected cell cycle functions. Compare peaks of predicted Cdc28p targets (26) vs. peaks of *CDC28* (*D*).

replication and the second in G_2/M phase (the functional significance of this second wave is unknown) (Fig. 4*C*). Another example is *CDC28*, discussed below (SI Fig. 10). Secondary peaks of CCTR genes suggest that they may function at multiple moments of the cell cycle or that only one of the observed peaks is cell cycle-related. Examples of calculated peaks are shown in

Fig. 4*D* and in Table 4 of *SI Appendix* (for the full list, see Table 6 in *SI Appendix* or http://cellcycle.info).

CCTR Genes. The timing results can only be interpreted within the context of cell cycle-regulated expression if a gene is CCTR. To identify CCTR genes, we examined available whole-genome data sets in which known cell cycle-regulated genes exhibited modulation (1, 3, 5, 14). For each transcript, we constructed a probabilistic score based on the percentage of earlier proposed (1, 5) cell cycle transcriptionally regulated genes among the 100 most correlated in each data set (1, 3, 5, 14) (see *SI Appendix*). This score identified a high-confidence CCTR set consisting of 694 genes and an extended set of 1,129 genes (see Table 6 in *SI Appendix*). We validated these CCTR sets by using experimental transcription factor binding data (11, 20, 21), as well as transcription factor binding motifs conserved among related fungi species (22, 23). Both tests showed that our CCTR sets are more consistent with independent transcription regulation data than are sets derived from smaller groups of experiments (3, 5) (see Tables 1 and 2 in *SI Appendix*). Henceforth, the term "CCTR genes" refers to the high-confidence set.

Error Estimation. To estimate the robustness of the timing procedure, we have investigated the extent to which the obtained peak times are affected by expected errors in the measured mRNA concentrations (see *SI Appendix*). We confirmed that the timing method is very robust; the median value of estimated total error for predicted peak times is 2 min (see Table 6 in *SI Appendix*). Such high-accuracy timing allows annotating of each transcript to a small fraction of a cell cycle phase and reveals otherwise undetectable differences in gene expression times. The complete list of CCTR genes, together with their expression peaks and error estimates, is available online at http://cellcycle.info.

Phase and Subphase Assignment. We defined time intervals corresponding to the main cell cycle phases (Fig. 4*E*) by using expression peaks of known cell cycle genes (see Table 5 in *SI Appendix*). The histogram of expression peaks of CCTR genes (Fig. 4*F*) reveals two main waves of transcription, separated by intervals of almost no CCTR transcriptional activity, between late S and late G_2 phases and in most of the G_1 phase. This dramatic variation in transcriptional activity between stages of the cell cycle has not been described previously (5) (SI Fig. 6). Beyond prominent expression waves in G_1/S–S and G_2/M–M, the histogram in Fig. 4*F* reveals a previously unidentified (1, 3, 5), distinct expression wave preceding the start of DNA replication. In YMC, this wave spans 45 min and encompasses 19% of CCTR genes. Because the majority of subunits of the prereplicative complex are expressed in this phase (Fig. 4*A*), we propose to designate it the "prereplicative" or "G_1 (P)" phase. Other genes expressed in G_1 (P) are involved in preparation for budding (e.g., *RSR1*, *BUD13*, *GIC2*, *RAX1*, *PEA2*, and *BNI4*) and in synthesis of cell wall components (e.g., *FKS1*, *GAS1*, and *GAS5*). In previous studies, G_1 (P) genes were perhaps incorrectly assigned to different cell cycle phases (1, 5). More than one-third had been annotated as being expressed in mitosis or M/G_1 (1, 5), including all subunits of the MCM complex and the G_1 cyclin *CLN3* (1, 5). Our timing places expression of these genes at the beginning of the new cycle, suggesting involvement in preparation for a round of division rather than for entry into extended G_1 phase, which is more consistent with their known biological function (6, 24).

Another gene expressed in G_1 (P) phase is *CDC28*, the catalytic subunit of the main yeast cyclin-dependent kinase, which drives progress through the cell cycle (25). Our study, which classifies *CDC28* as periodic, challenges the established view (3, 5, 8, 12, 25) that *CDC28* is constitutively expressed. We determined that *CDC28* expression peaks twice per cycle, first in G_1 (P) phase and again in early mitosis (Fig. 4*C*), precisely coinciding with expression waves of its predicted targets (26) (Fig. 4*H*). The periodicity of *CDC28* expression in YMC is strikingly clear (SI Fig. 10; $P < 0.00003$); it also is not an artifact of metabolic regulation, because a similar profile of *CDC28* had been earlier observed under different cell cycle synchronization (1) (SI Fig. 5). The lack of earlier acceptance of *CDC28* as transcriptionally regulated seems to be rather an artifact of the Fourier methods used (3, 5, 8), which, although convenient, are unable to deal appropriately with genes expressed twice per cycle (see *SI Appendix*).

Our timing results have also clarified when some key cell cycle genes are expressed. For instance, on the basis of experiments with rapidly growing yeast (1, 5), *CLB1*, *SWI5*, and *CLN3* have all been thought to be expressed during mitosis (1, 5), whereas our data suggest that G_2 cyclin *CLB1* is expressed in G_2, *SWI5* in G_2/M, and *CLN3* upon reentry to the cell cycle, in G_1 (P) (see Fig. 2). Similarly, we find that the Swi5-activated cyclin, *PCL9*, is expressed in mitosis and *MCM3* is expressed in G_1 (P), and consequently their expression can be delayed by an arbitrarily long G_1 phase, although, on the basis of experiments with rapidly growing yeast (1, 5), they were both believed to be expressed in M/G_1 (Fig. 2). Our timing results consistently place the expression of these key genes just before the time their products are needed within the cell cycle (6, 24).

Initiation of DNA Replication. The initiation of DNA replication occurs at the beginning of S phase and requires the prior assembly and subsequent modifications of the prereplicative complex (24), which starts in G_1 (P) (Fig. 4*B*). Strikingly, our timing of the expression peaks of CCTR subunits of MCM, replicative complex and elongation complex, corresponds with the exact order in which their gene products are needed (Fig. 4 *A* and *B*). The subunits of the origin of replication complex, *ORC2–6*, have not previously been classified as transcriptionally regulated, nor did they pass the stringent criteria of being accepted as CCTR in this study. Still, applying the deconvolution timing to their expression profiles reveals that these genes have expression peaks ≈10 min before the MCM subunits, exactly when their products are needed. This observation raises the possibility that the transcription of *ORC2–6* is regulated as a function of the cell cycle, contrary to established beliefs (1, 3, 5, 8) (Fig. 4*A*).

A more detailed view reveals that subunits of the MCM complex are expressed in two groups of three, separated by an ≈8-min interval, with each predicted expression group containing one MCM subunit with a nuclear localization signal (27) (Fig. 4*A*). These results may provide insight into the dynamics of MCM complex assembly and transport from cytoplasm into nucleus (28).

The precision of our timing data reveals that the SBF- and MBF-activated expression programs, thought to be identically timed during the mitotic cell cycle (29), actually differ (Fig. 4*G*). Unlike MBF, whose targets peak predominantly in G_1/S phase, targets of SBF are also activated in G_1 (P) phase and are generally characterized by a broader time distribution (Fig. 4*G*). This conclusion holds, independent of whether SBF and MBF targets are defined based on evolutionary analysis of conserved binding sites in 17 related fungus species or on various experimental studies (29, 30).

Cell Cycle-Regulated Complexes. We also timed expression of several other complexes, such as the spindle pole body (SPB) (Fig. 4*C*) (see Table 5 in *SI Appendix*). We observed especially tight transcriptional coregulation for complexes active in late G_1 and S phase; the elapsed time between expression peaks of the first and last CCTR subunits of a complex is between 5 min

(RFA) and 22 min (histones) (Fig. 4*C*). Transcription of many non-CCTR subunits of the cell cycle complexes also exhibits variability, allowing for timing, albeit weak. For example, only three subunits of RFC are CCTR, although expression of all five subunits occurs in the same 12-min interval (Fig. 4*C*). *ORC2–6* exhibit even weaker modulation, but interestingly their expression timing is nevertheless very consistent with the time in which they function (Fig. 4 *A* and *B*). The anaphase-promoting complex (APC) contains only two CCTR subunits, although the expression peaks of most of its 16 subunits appear in a time interval broadly corresponding to mitosis (Fig. 4*C*). However, some APC subunits, e.g., Cdh1, seem to be only posttranscriptionally regulated (31).

We generally find more subunits of the cell cycle-involved complexes to be CCTR than was the case in previous studies (2, 5, 8) (Fig. 4 and see *SI Appendix* and http://cellcycle.info). This difference may be explained by the increased quantity and improved accuracy of cell cycle expression data, together with our comprehensive approach to identifying CCTR genes. In addition to the examples discussed above and complexes involved in DNA replication initiation, we find more components of the septin ring of the mother-bud neck to be CCTR. Previous studies (2, 3, 5, 8) each classified only one septin (either *CDC11* or *CDC10*) as cell cycle-regulated, whereas we classify three components of the septin ring (*CDC11*, *CDC12*, and *CDC3*) as CCTR. Our classification of *CDC11*, *CDC12*, and *CDC3* as coregulated is independently supported by timing results (not used for classification), which places their expression peaks within an ≈6-min interval in late S phase.

Discussion

Until now, the cell cycle has been studied in logarithmically growing yeast cultures, in which virtually every cell divides during each oscillation (1, 3, 5). In the YMC, only about half of the cells divide in every oscillation of the culture (14). Consequently, the average expression levels of the CCTR genes in the YMC culture may be expected to be lower than in logarithmically growing cultures. However, because our analysis does not depend on absolute fold-change ratios, the fact that only half of the population goes through a cell cycle is not a hindrance. Furthermore, the YMC system offers many advantages, including stable synchronization and slow growth, that allow us to better distinguish between consecutive stages of the cell cycle.

It is possible, however, that some of the CCTR genes periodic in the YMC are regulated as a part of the metabolic oscillation, independent of the cell cycle. Therefore, we have used expression patterns from all budding yeast cell cycle data sets for classification of genes as CCTR. Still, the YMC condition increases the number of genes in our CCTR set, but we view this as a reflection of the cell cycle under a different set of natural conditions, rather than as an artifact of metabolically induced synchrony.

In previous cell cycle studies, two types of synchrony have been used (32–34): (*i*) induced synchrony, which forces cells to synchronize by some intervention such as pheromone arrest or the use of temperature-sensitive *cdc* mutants, and (*ii*) selection synchrony, which selects a cohort of cells at the same cell cycle stage, as in the elutriation method. Although it has been argued that selection methods are theoretically superior (35), so far for budding yeast they have resulted in whole-genome cell cycle data of inferior quality as compared with the intervention method (5). The cell cycle synchronization method we use here is of a third type. It is more a natural state of metabolic synchrony than an intervention method because, although an initial starvation is necessary to induce YMC synchrony, unlike in all other intervention methods (1, 5, 32), the synchrony remains stable (14).

How is the timing of gene expression that we describe here mirrored at the level of proteins? The key factor here is protein half-life: the more short-lived the protein, the closer the protein concentration correlates with transcript concentration. A recent whole-genome study of protein half-lives in budding yeast (36) reports that known cell cycle proteins are especially short-lived. These data show as well that our CCTR set is significantly enriched in rapidly degraded proteins, confirming that studying the timing of CCTR gene expression is a valuable proxy for understanding the temporal orchestration of the cell cycle proteome.

The deconvolution-based timing method we developed can also be applied to cell cycle data from other species (1, 4, 13, 37–39) and to analysis of other temporal phenomena with models of cell population synchrony, such as those during circadian rhythms (40) or development (41). One can judge the potential advantages of applying our methods by examining the power spectrum of the temporal profiles in question. The advantages of applying deconvolution will be greatest when squared magnitudes of discrete Fourier modes corresponding to multiplicities of the primary frequency are a measurable contribution to the power spectrum.

In summary, the precise timing of gene expression, using data from a highly synchronized continuous culture, has revealed the sequence of cell division events in fine detail, thereby providing a reference for defining cell cycle stages and studying individual gene functions. We have observed a prereplicative expression wave, occurring at the crucial time before the start of DNA replication. Our work has also enriched the description of eukaryotic cell cycle transcription, supplying detailed information on cell cycle progress under nutrient-poor conditions, which are perhaps more reflective of natural yeast growth conditions in the wild. From our analysis, we infer that just-in-time transcription is more prevalent in cell cycle regulation than previously recognized. The confinement of expression of genes sharing the same function to specific time intervals within the cycle (Fig. 4*H*) can be helpful in predicting gene function (SI Fig. 9). Moreover, the striking correlation between genes having a related function and the timing of their expression could result from the need for economical use of transcripts and proteins. Although phenotypes corresponding to the loss of such temporal optimizations could be difficult to observe, they might still be subject to natural selection in species such as yeast, which have a large effective population size.

Methods

Typical Profile Shape. To correct for the influence of imperfect cell cycle synchrony on measured mRNA concentrations, we modeled the time-shift distribution of cells entering the cell cycle. Using the common profile, we describe the time-shift distribution as an exponent of a fourth-degree polynomial, with the full width at half maximum of 48 min (see *SI Appendix*).

Deconvolution Algorithm. The measured profile, M, is the convolution of the individual cell profile, f, with the time-shift distribution h:

$$M(t) = \int f(t-\tau)h(\tau)\mathrm{d}\tau.$$

To find f, we optimize the following functional consisting of goodness-of-fit and regularization terms:

$$\sum_i \left((M(t_i) - \int f(t_i-\tau)h(\tau)\mathrm{d}\tau)/\sigma(t_i) \right)^2$$

$$+ A \int f(\tau)\ \log f(\tau)\mathrm{d}\tau,$$

where the sum is over all measurements, A corresponds to the amount of regularization applied, and σ is the expected error of each measurement (see *SI Appendix* and SI Fig. 7).

Timing. For each of the CCTR genes, we calculated the deconvolved profiles and identified the peaks of expression. Significant peaks were selected based on a heuristic score that included peak height, width, and shape (see *SI Appendix*). Using deconvolved gene expression profiles, we were able to observe secondary (lower-scoring) expression peaks, even when they were not evident in the raw data.

Error Estimation. To estimate the robustness of the timing procedure, we have investigated the extent to which the obtained peak times are affected by expected errors in the measured mRNA concentrations. Using Monte Carlo simulations (3,456 mock microarrays) we estimated the accuracy of peak time determination for all predicted CCTR genes (see *SI Appendix*). We confirmed that the timing method is very robust; the median value of estimated total error for predicted peak times is ≈2 min.

Physiological Time. To align precisely the three measured cycles in the YMC (which vary in length up to 11.5 min), we converted all measurement times into physiological time, using the rapid changes in dissolved oxygen concentrations as a reference (see SI Fig. 7 and *SI Appendix*). Thus, every measurement is assigned a physiological time between 0 and 300 min, with minute 0 corresponding to the point of maximal dissolved oxygen consumption. The resulting correction in timing is relatively small. To correct for residual long-term changes, logarithmic detrending has been applied to transcript concentrations. All timing results presented in *SI Appendix* and Fig. 4 are expressed in physiological time.

The gene expression data used for gene timing were provided by the laboratory of S.L.M. in the Department of Biochemistry at University of Texas Southwestern Medical Center. We thank G. Sherlock for the complete aggregate score for the Spellman *et al.* (5) data; J. Ihmels, N. Barkai, and A. Tanay for making available their sequence data; and A. Pertsemlidis, C. Wojcik, S. Altschuler, and L. Wu for helpful suggestions. This work was supported by National Institutes of Health Grant GM 74942 (to Z.O., M.R., and A.K.) and a Helen Hay Whitney Foundation Postdoctoral Fellowship (to B.P.T.).

1. Cho RJ, Campbell MDI, Winzeler EA, Steinmetz L, Conway A, Wodicka L, Wolfsberg TG, Gabrielian AE, Landsman D, Lockhart DJ, Davis RW (1998) *Mol Cell* 2:65–73.
2. Cho RJ, Huang MX, Campbell MJ, Dong HL, Steinmetz L, Sapinoso L, Hampton G, Elledge SJ, Davis RW, Lockhart DJ (2001) *Nat Genet* 27:48–54.
3. Pramila T, Wu W, Miles S, Noble WS, Breeden LL (2006) *Genes Dev* 20:2266–2278.
4. Rustici G, Mata J, Kivinen K, Lio P, Penkett CJ, Burns G, Hayles J, Brazma A, Nurse P, Bahler J (2004) *Nat Genet* 36:809–817.
5. Spellman PT, Sherlock G, Zhang MQ, Iyer VR, Anders K, Eisen MB, Brown PO, Botstein D, Futcher B (1998) *Mol Biol Cell* 9:3273–3297.
6. Breeden LL (2003) *Curr Biol* 13:R31–R38.
7. Cohen BA, Mitra RD, Hughes JD, Church GM (2000) *Nat Genet* 26:183–186.
8. de Lichtenberg U, Jensen LJ, Brunak S, Bork P (2005) *Science* 307:724–727.
9. Han JD, Bertin N, Hao T, Goldberg DS, Berriz GF, Zhang LV, Dupuy D, Walhout AJ, Cusick ME, Roth FP, Vidal M (2004) *Nature* 430:88–93.
10. Jensen LJ, Jensen TS, de Lichtenberg U, Brunak S, Bork P (2006) *Nature* 443:594–597.
11. Simon I, Barnett J, Hannett N, Harbison CT, Rinaldi NJ, Volkert TL, Wyrick JJ, Zeitlinger J, Gifford DK, Jaakkola TS, Young RA (2001) *Cell* 106:697–708.
12. Zhao LP, Prentice R, Breeden L (2001) *Proc Natl Acad Sci USA* 98:5631–5636.
13. Whitfield ML, Sherlock G, Saldanha AJ, Murray JI, Ball CA, Alexander KE, Matese JC, Perou CM, Hurt MM, Brown PO, Botstein D (2002) *Mol Biol Cell* 13:1977–2000.
14. Tu BP, Kudlicki A, Rowicka M, McKnight SL (2005) *Science* 310:1152–1158.
15. Kudlicki A, Rowicka M, Otwinowski Z (2007) *Bioinformatics* 23:1559–1561.
16. Hartwell LH, Unger MW (1977) *J Cell Biol* 75:422–435.
17. Lord PG, Wheals AE (1980) *J Bacteriol* 142:808–818.
18. Raser JM, O'Shea EK (2005) *Science* 309:2010–2013.
19. Silver RN, Sivia DS, Gubernatis JE (1990) *Phys Rev B Condens Matter* 41:2380–2389.
20. Harbison CT, Gordon DB, Lee TI, Rinaldi NJ, Macisaac KD, Danford TW, Hannett NM, Tagne JB, Reynolds DB, Yoo J, *et al.* (2004) *Nature* 431:99–104.
21. MacIsaac KD, Wang T, Gordon DB, Gifford DK, Stormo GD, Fraenkel E (2006) *BMC Bioinformatics* 7:113.
22. Ihmels J, Bergmann S, Gerami-Nejad M, Yanai I, McClellan M, Berman J, Barkai N (2005) *Science* 309:938–940.
23. Tanay A, Regev A, Shamir R (2005) *Proc Natl Acad Sci USA* 102:7203–7208.
24. Tye BK (1999) *Annu Rev Biochem* 68:649–686.
25. Mendenhall MD, Hodge AE (1998) *Microbiol Mol Biol Rev* 62:1191–1243.
26. Ubersax JA, Woodbury EL, Quang PN, Paraz M, Blethrow JD, Shah K, Shokat KM, Morgan DO (2003) *Nature* 425:859–864.
27. Forsburg SL (2004) *Microbiol Mol Biol Rev* 68:109–131.
28. Nguyen VQ, Co C, Irie K, Li JJ (2000) *Curr Biol* 10:195–205.
29. Iyer VR, Horak CE, Scafe CS, Botstein D, Snyder M, Brown PO (2001) *Nature* 409:533–538.
30. Horak CE, Luscombe NM, Qian J, Bertone P, Piccirrillo S, Gerstein M, Snyder M (2002) *Genes Dev* 16:3017–3033.
31. Zachariae W, Schwab M, Nasmyth K, Seufert W (1998) *Science* 282:1721–1724.
32. Shedden K, Cooper S (2002) *Nucleic Acids Res* 30:2920–2929.
33. Novak B, Mitchison JM (1990) *J Cell Sci* 96:79–91.
34. Creanor J, Elliott SG, Bisset YC, Mitchison JM (1983) *J Cell Sci* 61:339–349.
35. Shedden K, Cooper S (2002) *Proc Natl Acad Sci USA* 99:4379–4384.
36. Belle A, Tanay A, Bitincka L, Shamir R, O'Shea EK (2006) *Proc Natl Acad Sci USA* 103:13004–13009.
37. Ishida S, Huang E, Zuzan H, Spang R, Leone G, West M, Nevins JR (2001) *Mol Cell Biol* 21:4684–4699.
38. Laub MT, McAdams HH, Feldblyum T, Fraser CM, Shapiro L (2000) *Science* 290:2144–2148.
39. Menges M, Hennig L, Gruissem W, Murray JA (2003) *Plant Mol Biol* 53:423–442.
40. Claridge-Chang A, Wijnen H, Naef F, Boothroyd C, Rajewsky N, Young MW (2001) *Neuron* 32:657–671.
41. Dequeant ML, Glynn E, Gaudenz K, Wahl M, Chen J, Mushegian A, Pourquie O (2006) *Science* 314:1595–1598.